Deep Learning-Based Aerosol and Ocean Data Retrieval from Satellite Polarimeter Measurements

Lingxiao Wang
Dept. of Electrical Engineering
Louisiana Tech University
Ruston, Louisiana, USA
lwang@latech.edu

Snorre Stamnes
NASA Langley Research Center
Hampton, Virginia, USA
snorre.a.stamnes@nasa.gov

Sunzid Hassan
Dept. of Computer Science
Louisiana Tech University
Ruston, Louisiana, USA
sha040@latech.edu

Alexander Isiani
Dept. of Electrical Engineering
Louisiana Tech University
Ruston, Louisiana, USA
aci004@latech.edu

Cheston Sturdivant
Dept. of Electrical Engineering
Louisiana Tech University
Ruston, Louisiana, USA
ccs060@latech.edu

Hoang My Le
Dept. of Electrical Engineering
Louisiana Tech University
Ruston, Louisiana, USA
hmy006@latech.edu

Khan Raqib Mahmud
Dept. of Computer Science
Louisiana Tech University
Ruston, USA
krm070@latech.edu

***Abstract*—This paper presents a deep learning (DL)-based approach for retrieving aerosol and ocean optical parameters from polarimeter measurements. The traditional data retrieval method, i.e., Microphysical Aerosol Properties from Polarimetry (MAPP) algorithm, involves vector radiative transfer (VRT) calculations, which are a time-consuming and computationally intensive process. To address this limitation, we propose replacing the VRT calculations in MAPP with DL models to accelerate the data retrieval process. The core idea is to train DL models to replicate VRT calculations used in MAPP. To achieve this, we collected 2 million input-output pairs from the VRT calculations in MAPP to construct a comprehensive training dataset. Three types of DL models, including feedforward neural networks (FNNs), convolutional neural networks (CNNs), and recurrent neural networks (RNNs), were developed to learn the underlying VRT calculation pattern through supervised learning. The performance of these models was evaluated using a test dataset, with the RNN model achieving the highest prediction accuracy. Experimental results indicate that the proposed DL-based approach can improve the data retrieval efficiency of MAPP algorithm while maintaining high accuracy in the data retrieval process.**

***Index Terms*—deep learning, passive remote sensing, polarimetry**

I. Introduction

Launched in 2024, the Plankton, Aerosol, Cloud, and Ocean Ecosystem (PACE) satellite is NASA's recent Earth observing satellite. Equipped with two multi-wavelength, multi-angle imaging polarimeters [1], PACE measures and monitors aerosol and ocean parameters, enabling environmental scientists to investigate the impacts of climate change on ocean phytoplankton blooms and understand how airborne particles, such as dust and smoke, influence cloud formation and the Earth's heating and cooling dynamics [2].

A conventional method for extracting aerosol and ocean parameters is the Microphysical Aerosol Properties from Polarimetry (MAPP) algorithm [3], which employs optimal estimation to iteratively fit a state vector of aerosol and ocean parameters by minimizing the difference between the estimated and observed polarimeter measurements. A key step in MAPP is to map the state vector to polarimeter measurements using vector radiative transfer (VRT) calculations. While effective, the major limitation of MAPP is its processing speed since solving VRT equations is computationally intensive, making the algorithm impractical for large-scale data retrieval tasks.

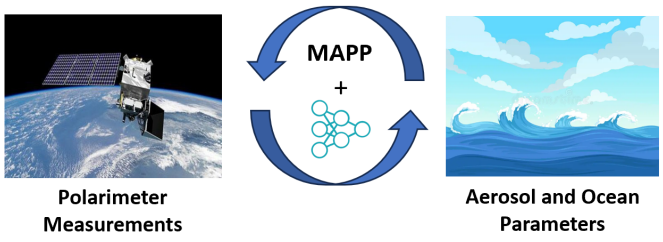

Fig. 1. The proposed Deep Learning (DL)-based satellite data retrieval method is designed to replace the vector radiative transfer (VRT) in the conventional data retrieval algorithm, MAPP [3], to accelerate the data retrieval time.

In this work, as illustrated in Fig. I, our objective is to replace the time-intensive VRT calculations in MAPP with deep learning (DL) techniques. Recent advancements in DL algorithms and computational hardware have established DL as a powerful tool for addressing complex problems across diverse domains, including image processing [4], [5], data prediction [6], [7], and robot control [8], [9]. The motivation for using DL techniques to replace VRT calculations lies in their significantly faster query times. For instance, the calculation time for MAPP in one cycle data retrieval takes 60 minutes [10], while the DL models' query time is less than 1 second. In addition, DL models can effectively replicate the functionality of VRT. Thus, this approach has the potential to transform data retrieval efficiency, making it scalable for large datasets and real-time applications.

The core of training a DL model lies in enabling it to learn a mapping function from provided input-output data pairs. To

SoutheastCon 2025 | 979-8-3315-0484-7/25/$31.00 ©2025 IEEE | DOI: 10.1109/SOUTHEASTCON56624.2025.10971488

Authorized licensed use limited to: Old Dominion University. Downloaded on January 27,2026 at 20:04:53 UTC from IEEE Xplore. Restrictions apply.

develop DL models capable of replicating the functionality of VRT calculations, we first generated a diverse training dataset by pre-running VRT calculations in MAPP with a variety of input state vectors. Each input and its corresponding output were recorded as input-output pairs, and a total of 2 million pairs were collected for the training dataset, with an additional 200,000 pairs collected for the testing dataset. Three types of DL models, including feedforward neural networks (FNNs), convolutional neural networks (CNNs), and recurrent neural networks (RNNs), were developed in this work. The proposed FNN, incorporated with multiple hidden layers, predicts the VRT calculation results based on a single input state vector. In contrast, the CNN and RNN architectures are designed to process multi-step input vectors, enabling them to predict VRT results while incorporating contextual information. We summarize the contributions of this work as follows:

- We developed three types of DL models, including FNN, CNN, and RNN, to replicate the functionality of VRT in the MAPP algorithm, accelerating the aerosol and ocean data retrieval process from satellite measurements;
- We prepared an extensive training dataset of 2 million input-output pairs, generated from pre-computed VRT calculations, and used it to train the developed DL models;
- We evaluated the trained DL models on an additional testing dataset containing 200,000 input-output pairs. Experimental results show that the proposed RNN, with the slide window of size 3, achieved the highest prediction accuracy.

The remainder of this paper is organized as follows: Section II reviews related works on data retrieval from polarimeters; Section III outlines the proposed DL-based models and details the training process; Section IV presents the results of the trained DL models on the testing dataset; and Section V discusses the conclusions and future research directions of this work.

II. Related Works

Aerosol and ocean data retrieval refers to the process of extracting information about atmospheric aerosols and ocean properties from satellite measurements [11]. In this data retrieval process, a forward model that maps aerosol and ocean properties into satellite measurements is a necessary step. Many existing data retrieval algorithms have modeled this forward model as VRT [3], [12]–[15]. However, VRT calculations are computationally intensive, making it challenging to apply these methods to large-scale data retrieval tasks. Therefore, a key research question naturally arises: can the time-consuming VRT calculations be replaced with a faster method while preserving the functionality and accuracy of VRT?

With advancements in DL algorithms and the increasing affordability of computational resources, the use of DL techniques for solving real-world challenges has become widespread. In image processing, CNNs have dominated object detection and image classification tasks for the past decade [16]–[18]. In natural language processing (NLP), RNNs and the recently developed Transformers [19] excel in text generation, translation, and sentiment analysis [20]. In robotics, DL-controlled robots can defeat human players in the game of Go [21] and can be utilized for path planning in autonomous driving tasks [22].

Inspired by these advancements and the ability of DL to replicate complex mapping functions, researchers have explored using DL techniques to replace computationally expensive VRT calculations, thereby accelerating the data retrieval process. For instance, the PACE-MAPP algorithm [23], designed to process polarimeter measurements from the PACE satellite, utilizes a four-layer FNN as the forward model to replace VRT calculations. Experimental results show that the developed FNN can accurately replicate VRT functionalities and decrease the overall data retrieval time. Similarly, Dommalapati et al. [10] employed an FNN to replace VRT calculations in the particulate matter (PM) retrieval from polarimeter measurements. Gao et al. [24] proposed the FastMAPOL algorithm, which replaces the VRT calculations with a FNN. In this work, various combinations of layers and nodes in the DL structure were investigated to optimize the prediction performance.

Compared to these existing DL-based efforts in satellite data retrieval, our work distinguishes itself in two ways: (i) Besides FNNs, we investigated more advanced DL architectures, including CNNs and RNNs, for replacing VRT calculations in satellite data retrieval tasks. While the use of DL models in this field has grown in popularity, previous works have largely focused on FNNs, with minimal exploration of CNNs and RNNs; (ii) Our models were trained on an extensive dataset of 2 million input-output pairs, significantly larger than the datasets used in prior studies, such as 120,000 pairs in [23]. This extensive dataset allows our models to capture a wider range of variations to ensure the generalization of the proposed DL models in various using scenarios.

III. Methodology

A. Problem Formation

The main task of this work is to design DL models, i.e., Deep Neural Networks (DNNs), to replicate the functionality of VRT calculations in the MAPP algorithm [3]. In MAPP, the data retrieval starts with an initial estimate of aerosol and ocean parameters, known as the state vector. These initial estimates are mapped to the polarimetry data using VRT calculations, and the resulting mapped polarimetry data is compared with observed (i.e., real) polarimetry data measurements. The difference between the estimated and observed data is then used to iteratively update the state vector. This iterative process continues until the gap falls within a predefined uncertainty threshold.

Polarimeter measurements consist of two key parameters: the Reflectance (R_I) and the Degree of Linear Polarization (DOLP). Both are vectors with 11 features each, resulting in a combined sensor measurement vector, $\mathbf{y} = [R_I, DOLP]$, containing 22 features. The state vector, $\mathbf{x}$, includes aerosol and ocean properties such as aerosol optical depth, marine

Authorized licensed use limited to: Old Dominion University. Downloaded on January 27,2026 at 20:04:53 UTC from IEEE Xplore. Restrictions apply.

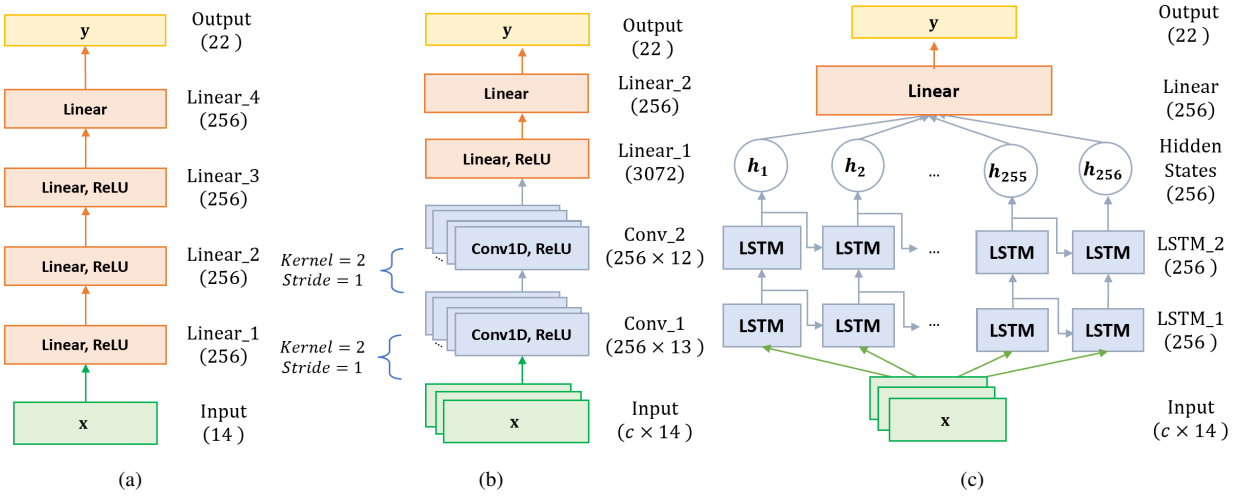

Fig. 2. The architecture of the proposed (a) FNN, (b) CNN, and (c) RNN models. For inputs of CNN and RNN, multiple inputs, i.e., c, are fed to the model to make a prediction. The FNN consists of three hidden layers, each containing 256 nodes, and an output layer, also with 256 nodes. For all DL models, the output layer generates outputs for the R_I and $DOLP$ features.

aerosol, and ocean surface roughness, totaling 11 features. For the MAPP algorithm, 3 additional solar-instrument observation geometries are included in the state vector, bringing the total to 14 features. The values in $\mathbf{x}$ are iteratively refined by minimizing the following cost function [3]:

$$\chi^2(\mathbf{x}) = \Phi(\mathbf{x})_{\text{data}} + \Phi(\mathbf{x})_{\text{prior}} = \frac{1}{2}[(\boldsymbol{f}-\mathbf{y})^T \mathbf{S}_\epsilon^{-1}(\boldsymbol{f}-\mathbf{y}) + (\mathbf{x}-\mathbf{x}_a)^T \mathbf{S}_a^{-1}(\mathbf{x}-\mathbf{x}_a)], \quad (1)$$

where $\boldsymbol{f}$ represents VRT calculations that map the state vector into polarimeter measurements, i.e., $\hat{\mathbf{y}} = \boldsymbol{f}(\mathbf{x})$; $\mathbf{x}_a$ is the *a priori* state vector, using the mean of the allowable range of each feature in $\mathbf{x}$; $\mathbf{S}_\epsilon$ and $\mathbf{S}_a$ are tuning matrices to adjust the weights of latest sensor measurements or initial parameter estimates, respectively. In this work, we seek to replace $\boldsymbol{f}$ with a DNN.

B. DNN Model Design

We begin with the simplest DL structure, i.e., FNN. The architecture of the proposed FNN, illustrated in Fig. 2(a), consists of an input layer, three hidden layers, and an output layer. Each layer contains 256 nodes, and 3 hidden layers include the ReLU activation function [25] to introduce non-linearity.

Compared to the FNN, both CNN and RNN architectures are designed to process the sequential data structure, enabling them to incorporate contextual information when making predictions. As shown in Fig. 2(b), the proposed CNN model begins with a convolutional block comprising two 1-dimensional convolutional layers. Each convolutional layer has 256 nodes, a kernel size of 2, and a stride of 1. Following the convolutional layers, the output is flattened and passed through a fully connected block consisting of one hidden layer with the ReLU activation function and an output layer.

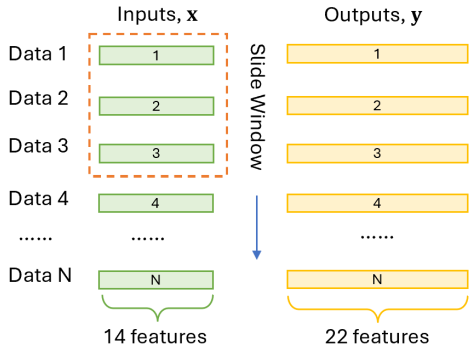

Fig. 3. The dataset is fed to DNNs using a sliding window, where the CNN and RNN models are trained using c sequential input entry to predict 1 output entry, while the FNN model is trained using 1 sequential input data to predict 1 output entry. Here, c is the length of slide window.

For the RNN model, we utilize a Long Short-Term Memory (LSTM) architecture. As depicted in Fig. 2(c), the architecture starts with an input layer that processes sequences of aerosol and ocean parameter data. The input is passed through two stacked recurrent layers equipped with LSTM memory cells, which are capable of learning both short- and long-term dependencies in the data [26]. The encoded representation is then fed into a fully connected layer, which integrates the learned features and produces the output predictions.

C. Training Details

1) Training Data Collection: The training data was obtained by using VRT calculations in MAPP with the provided input state vectors. Here, we generate simulated state vectors and then use the forward model (i.e., VRT) in MAPP to calculate the result. The simulated input state vector was obtained from a uniform distribution of realistic state parameter to create a set of diverse yet plausible state vectors. Then,

Authorized licensed use limited to: Old Dominion University. Downloaded on January 27,2026 at 20:04:53 UTC from IEEE Xplore. Restrictions apply.

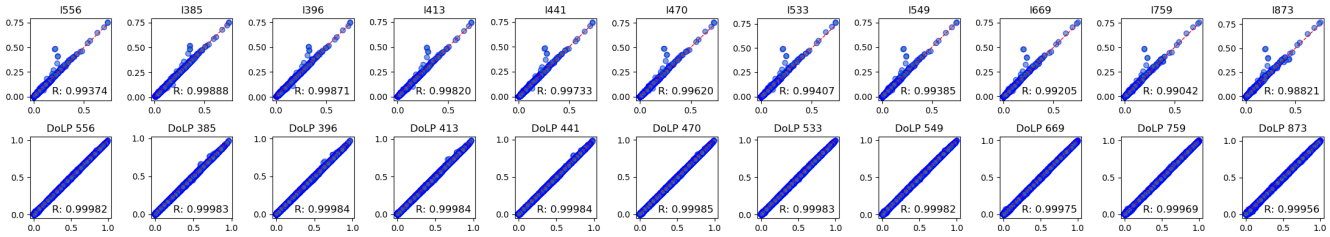

(a) FNN

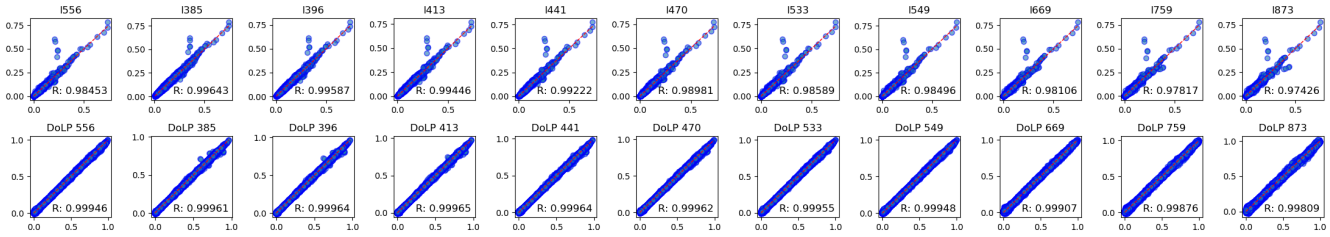

(b) CNN

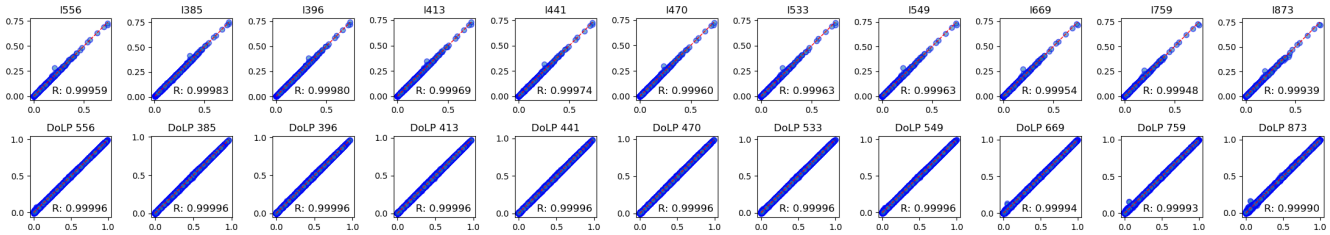

(c) RNN

Fig. 4. Parity plots of (a) FNN, (b) CNN, and (c) RNN models evaluated on the testing dataset, each using 200,000 data inputs. The horizontal axis represents the ground truth values generated from VRT calculations, while the vertical axis represents the predicted values from the DL models. For each sub-figure, the first row of diagrams corresponds to R_I across 11 channels, and the second row corresponds to $DOLP$ across 11 channels. The R^2 value is displayed at the bottom of each parity plot, where the R^2 score approaching to 1 indicates higher prediction accuracy.

these state vectors are fed to the VRT model to calculate the estimated polarimeter measurements, which are treated as labels for the input vectors. Using this approach, we created 2 million input-output vector pairs. For testing, we generate an additional 200,000 pairs of data, which are hidden during the training process.

2) Training Data Preparation: The training data preparation process differs for the FNN and CNN/RNN models due to their architectural capabilities. Since CNN and RNN models can process multi-step input vectors, we implemented a sliding window approach (as shown in Fig. 3) for these models, allowing multiple input instances to be included in each training step. The length of the sliding window, denoted as c, is a tuning parameter. During the training process, we experimented with three different values for c, including 3, 10, and 100, and found that the model has the best prediction performance when $c = 3$. In contrast, the FNN model processes single-step input vectors, making the sliding window size equal to 1.

The sliding window moves sequentially through the dataset, capturing overlapping data instances for training. During training, all DL models were trained with a batch size of 256. Consequently, the input data size for the FNN model is $(256, 14)$, representing 256 single-step vectors with 14 features each. For CNN and RNN models, the input data size is $(256, c, 14)$, capturing c sequential instances with 14 features per instance. The output of the all models has the same dimension of $(256, 22)$, where 22 is the size of output vector $\mathbf{y}$.

3) Training Parameters: The models were implemented in PyTorch [27] and trained using the mean squared error (MSE) as the loss function, which is calculated via:

$$MSE = \frac{1}{N}(\hat{\mathbf{y}} - \mathbf{y})^2, \tag{2}$$

where N is the batch size, i.e., 256 in this project, $\hat{\mathbf{y}}$ is the DL model output, and $\mathbf{y}$ is the ground truth value, i.e., the result of VRT calculations. The optimization method was selected as Adam with the learning rate of 10^{-5}. The training process was configured with a maximum of 200 epochs, and an early stopping was applied if the model's performance did not improve for 20 consecutive epochs.

All three models were trained on a workstation equipped with an Intel 14900KF i9 CPU, NVIdIA RTX 4080 Super GPU, and 32 GB of RAM. GPU acceleration was enabled

Authorized licensed use limited to: Old Dominion University. Downloaded on January 27,2026 at 20:04:53 UTC from IEEE Xplore. Restrictions apply.

TABLE I
MSE OF DL MODELS ON TESTING DATASET

	Window Size c	MSE ↓
FNN	-	0.00459
CNN	3	0.01415
	10	0.01491
	100	0.02299
RNN	**3**	**0.00098**
	10	0.00181
	100	0.00119

during the training process, and the training times for the FNN, CNN, and RNN models were approximately 2 hours, 2.5 hours, and 4 hours, respectively.

IV. EXPERIMENTS AND RESULTS

A. Determine Slide Window Size

All models were evaluated using the testing dataset, which contains 200,000 input-output pairs. This testing dataset is hidden to the model during the training process. For the proposed CNN and RNN, we tried different slide window size (c) to determine the optimal value. Specifically, we set the slide window with three different sizes: $c = 3$, $c = 10$, and $c = 100$. This results in six DL models, three for CNN and three for RNN. Table I presents the total MSE of all 22 output features on the testing dataset for each model. As shown in the table, the window size of 3 achieves the highest prediction accuracy for both CNN and RNN, as indicated by the lowest total MSE compared to other window sizes.

From Table I, we can also observe that the proposed RNN with window size of 3 achieves the highest prediction accuracy among all tested configurations, outperforming FNN and both CNN and RNN models with other window sizes. For the RNN with slide window size of 3, the MSE is 0.00098, which is 93.1% less than the best CNN model and 78.6% less than the FNN model.

B. Parity Plots on Prediction v.s. Ground Truth

Detailed prediction results on each output feature are provided in Fig. 4, which presents the parity plots for the three proposed DL models. Here, both RNN and CNN have a slide window size of 3. For each model, the first row of diagrams is related to R_I, and the second row of diagrams corresponds to $DOLP$, with each having 11 channels, totaling 22 parity plots per model. In all parity plots, the horizontal axis represents the ground truth values derived from VRT calculations, while the vertical axis shows the predictions made by the DL models, given the same input vectors. An R^2 score [28] is calculated for each parity plot to measure the correlation between predicted and ground truth values. The R^2 score closer to 1 indicates higher prediction accuracy.

From Fig. 4, it can be observed that all three models achieved relatively high prediction accuracy, as indicated by the scatter points being generally close to the 45-degree diagonal line. Specifically, the FNN and CNN models demonstrated better prediction accuracy on the $DOLP$ features compared to the R_I features, as evidenced by several outliers in the first 11 outputs of their parity plots. In contrast, the RNN model achieved the best overall prediction performance, with scatter points in all plots closely aligning with the 45-degree diagonal line, indicating the consistent prediction accuracy across all features.

This observation is further supported by the R^2 scores for FNN, CNN, and RNN. For instance, in the first channel of R_I, the R^2 score for FNN is 0.99374, while the CNN and RNN achieve 0.98453 and 0.99959, respectively. The RNNs R^2 score is closer to 1 compared to other models. This trend holds true for all R^2 scores across 22 outputs, with the RNN consistently achieving scores closer to 1.

The better performance of the RNN model can be attributed to its ability to effectively capture sequential and contextual information in the input data. Unlike FNN and CNN models, RNNs are specifically designed to handle sequential data by maintaining a hidden state that captures information from previous steps in the sequence. This configuration allows the RNN to learn patterns across multiple input instances. In this work, the RNN model was able to retain and integrate information across multiple input vectors within the sliding window, capturing the contextual information while making the prediction. The capability of using contextual information from sequential input data results in more accurate predictions for the RNN in both R_I and $DOLP$ predictions.

V. CONCLUSION AND FUTURE WORKS

This paper presents a DL-based method to replace the time-consuming VRT calculations in the traditional MAPP algorithm. The core idea is to train DL models to learn the underlying patterns of VRT. To achieve this, we prepared a dataset with various input vectors and their corresponding VRT outputs, with a total size of 2 million input-output pairs. We developed three types of models: FNN, CNN, and RNN. The FNN predicts based on single-step inputs, while the CNN and RNN process multi-step inputs, leveraging contextual information. The models were evaluated on an unseen testing dataset, and the evaluation performance was measured via MSE and R^2 scores. Results show that the DL models effectively replicate VRT calculations, with low MSE and high R^2. Among them, the RNN with a sliding window of 3 achieved the best performance across all 22 output features, outperforming FNN and CNN. These findings demonstrate the potential of DL models to replace VRT calculations in MAPP to enhance the efficiency and scalability of satellite data retrieval.

Future work for this study includes developing DL models to incorporate data from additional Earth-observing sensors. In this work, only polarimeter measurements were used for data retrieval. However, Lidar sensors are also widely employed in Earth observation tasks [29], which can offer complementary altitude-resolved information to the polarimeter measurements. Incorporating Lidar sensor measurements into DL-based data retrieval is an important topic for future research, enabling

Authorized licensed use limited to: Old Dominion University. Downloaded on January 27,2026 at 20:04:53 UTC from IEEE Xplore. Restrictions apply.

more comprehensive and robust retrieval capabilities. Additionally, exploring advanced DL architectures, such as Transformers, could further enhance the prediction performance. Like RNNs, Transformers can process multi-instance input sequences, allowing them to capture complex dependencies in the data. This capability has been well-established in natural language processing tasks, but its effectiveness in satellite data retrieval remains an area for further investigation. Finally, applying the proposed DL models to actual data retrieval tasks within the MAPP framework is another future research direction, which bridges the gap between experimental models and real-world satellite data retrieval applications.

ACKNOWLEDGMENT

This work is supported by the REA grant, Louisiana Board of Regents LaSPACE, under the contract PO-0000280099.

REFERENCES

[1] L. A. Remer, K. Knobelspiesse, P.-W. Zhai, F. Xu, O. V. Kalashnikova, J. Chowdhary, O. Hasekamp, O. Dubovik, L. Wu, Z. Ahmad *et al.*, "Retrieving aerosol characteristics from the pace mission, part 2: multi-angle and polarimetry," *Frontiers in Environmental Science*, vol. 7, p. 94, 2019.

[2] F. Waquet, B. Cairns, K. Knobelspiesse, J. Chowdhary, L. D. Travis, B. Schmid, and M. Mishchenko, "Polarimetric remote sensing of aerosols over land," *Journal of Geophysical Research: Atmospheres*, vol. 114, no. D1, 2009.

[3] S. Stamnes, C. Hostetler, R. Ferrare, S. Burton, X. Liu, J. Hair, Y. Hu, A. Wasilewski, W. Martin, B. Van Diedenhoven *et al.*, "Simultaneous polarimeter retrievals of microphysical aerosol and ocean color parameters from the "mapp" algorithm with comparison to high-spectral-resolution lidar aerosol and ocean products," *Applied optics*, vol. 57, no. 10, pp. 2394–2413, 2018.

[4] S. Minaee, Y. Boykov, F. Porikli, A. Plaza, N. Kehtarnavaz, and D. Terzopoulos, "Image segmentation using deep learning: A survey," *IEEE transactions on pattern analysis and machine intelligence*, vol. 44, no. 7, pp. 3523–3542, 2021.

[5] S. S. A. Zaidi, M. S. Ansari, A. Aslam, N. Kanwal, M. Asghar, and B. Lee, "A survey of modern deep learning based object detection models," *Digital Signal Processing*, vol. 126, p. 103514, 2022.

[6] J. F. Torres, D. Hadjout, A. Sebaa, F. Martínez-Álvarez, and A. Troncoso, "Deep learning for time series forecasting: a survey," *Big Data*, vol. 9, no. 1, pp. 3–21, 2021.

[7] K. Benidis, S. S. Rangapuram, V. Flunkert, Y. Wang, D. Maddix, C. Turkmen, J. Gasthaus, M. Bohlke-Schneider, D. Salinas, L. Stella *et al.*, "Deep learning for time series forecasting: Tutorial and literature survey," *ACM Computing Surveys*, vol. 55, no. 6, pp. 1–36, 2022.

[8] V. Mnih, K. Kavukcuoglu, D. Silver, A. A. Rusu, J. Veness, M. G. Bellemare, A. Graves, M. Riedmiller, A. K. Fidjeland, G. Ostrovski *et al.*, "Human-level control through deep reinforcement learning," *nature*, vol. 518, no. 7540, pp. 529–533, 2015.

[9] B. Singh, R. Kumar, and V. P. Singh, "Reinforcement learning in robotic applications: a comprehensive survey," *Artificial Intelligence Review*, vol. 55, no. 2, pp. 945–990, 2022.

[10] A. Dommalapati, A. Ranasinghe, J. Peele, S. Whetzel, M. Jones, A. Bell, E. Chemyakin, S. Stamnes, and H. Shakeri, "A neural-network-based forward model to improve air quality estimation from spaceborne polarimeters," in *2022 Systems and Information Engineering Design Symposium (SIEDS)*. IEEE, 2022, pp. 217–222.

[11] S. Zhang, J. Wu, W. Fan, Q. Yang, and D. Zhao, "Review of aerosol optical depth retrieval using visibility data," *Earth-Science Reviews*, vol. 200, p. 102986, 2020.

[12] P.-W. Zhai, Y. Hu, J. Chowdhary, C. R. Trepte, P. L. Lucker, and D. B. Josset, "A vector radiative transfer model for coupled atmosphere and ocean systems with a rough interface," *Journal of Quantitative Spectroscopy and Radiative Transfer*, vol. 111, no. 7-8, pp. 1025–1040, 2010.

[13] P.-W. Zhai, Y. Hu, D. M. Winker, B. A. Franz, J. Werdell, and E. Boss, "Vector radiative transfer model for coupled atmosphere and ocean systems including inelastic sources in ocean waters," *Optics express*, vol. 25, no. 8, pp. A223–A239, 2017.

[14] M. Gao, P.-W. Zhai, B. Franz, Y. Hu, K. Knobelspiesse, P. J. Werdell, A. Ibrahim, F. Xu, and B. Cairns, "Retrieval of aerosol properties and water-leaving reflectance from multi-angular polarimetric measurements over coastal waters," *Optics Express*, vol. 26, no. 7, pp. 8968–8989, 2018.

[15] L. Li, O. Dubovik, Y. Derimian, G. L. Schuster, T. Lapyonok, P. Litvinov, F. Ducos, D. Fuertes, C. Chen, Z. Li *et al.*, "Retrieval of aerosol components directly from satellite and ground-based measurements," *Atmospheric Chemistry and Physics*, vol. 19, no. 21, pp. 13 409–13 443, 2019.

[16] A. Krizhevsky, I. Sutskever, and G. E. Hinton, "Imagenet classification with deep convolutional neural networks," in *Advances in Neural Information Processing Systems*, F. Pereira, C. Burges, L. Bottou, and K. Weinberger, Eds., vol. 25. Curran Associates, Inc., 2012. [Online]. Available: https://proceedings.neurips.cc/paper_files/paper/2012/file/c399862d3b9d6b76c8436e924a68c45b-Paper.pdf

[17] K. Simonyan, "Very deep convolutional networks for large-scale image recognition," *arXiv preprint arXiv:1409.1556*, 2014.

[18] K. He, X. Zhang, S. Ren, and J. Sun, "Deep residual learning for image recognition. arxiv e-prints," *arXiv preprint arXiv:1512.03385*, vol. 10, 2015.

[19] A. Vaswani, "Attention is all you need," *Advances in Neural Information Processing Systems*, 2017.

[20] M. Zhou, N. Duan, S. Liu, and H.-Y. Shum, "Progress in neural nlp: modeling, learning, and reasoning," *Engineering*, vol. 6, no. 3, pp. 275–290, 2020.

[21] D. Silver, A. Huang, C. J. Maddison, A. Guez, L. Sifre, G. Van Den Driessche, J. Schrittwieser, I. Antonoglou, V. Panneershelvam, M. Lanctot *et al.*, "Mastering the game of go with deep neural networks and tree search," *nature*, vol. 529, no. 7587, pp. 484–489, 2016.

[22] Y. Hu, J. Yang, L. Chen, K. Li, C. Sima, X. Zhu, S. Chai, S. Du, T. Lin, W. Wang *et al.*, "Planning-oriented autonomous driving," in *Proceedings of the IEEE/CVF Conference on Computer Vision and Pattern Recognition*, 2023, pp. 17 853–17 862.

[23] S. Stamnes, M. Jones, J. G. Allen, E. Chemyakin, A. Bell, J. Chowdhary, X. Liu, S. P. Burton, B. Van Diedenhoven, O. Hasekamp *et al.*, "The pace-mapp algorithm: Simultaneous aerosol and ocean polarimeter products using coupled atmosphere-ocean vector radiative transfer," *Frontiers in Remote Sensing*, vol. 4, p. 1174672, 2023.

[24] M. Gao, B. A. Franz, P.-W. Zhai, K. Knobelspiesse, A. M. Sayer, X. Xu, J. V. Martins, B. Cairns, P. Castellanos, G. Fu *et al.*, "Simultaneous retrieval of aerosol and ocean properties from pace harp2 with uncertainty assessment using cascading neural network radiative transfer models," *Atmospheric Measurement Techniques*, vol. 16, no. 23, pp. 5863–5881, 2023.

[25] A. Agarap, "Deep learning using rectified linear units (relu)," *arXiv preprint arXiv:1803.08375*, 2018.

[26] S. Hochreiter, "Long short-term memory," *Neural Computation MIT-Press*, 1997.

[27] A. Paszke, S. Gross, F. Massa, A. Lerer, J. Bradbury, G. Chanan, T. Killeen, Z. Lin, N. Gimelshein, L. Antiga *et al.*, "Pytorch: An imperative style, high-performance deep learning library," *Advances in neural information processing systems*, vol. 32, 2019.

[28] D. Chicco, M. J. Warrens, and G. Jurman, "The coefficient of determination r-squared is more informative than smape, mae, mape, mse and rmse in regression analysis evaluation," *Peerj computer science*, vol. 7, p. e623, 2021.

[29] J. S. Schlosser, S. Stamnes, S. P. Burton, B. Cairns, E. Crosbie, B. Van Diedenhoven, G. Diskin, S. Dmitrovic, R. Ferrare, J. W. Hair *et al.*, "Polarimeter+ lidar–derived aerosol particle number concentration," *Frontiers in Remote Sensing*, vol. 3, p. 885332, 2022.

Authorized licensed use limited to: Old Dominion University. Downloaded on January 27,2026 at 20:04:53 UTC from IEEE Xplore. Restrictions apply.